RSC Advances

ROYAL SOCIETY OF CHEMISTRY

www.rsc.org/advances

Journal Name

ARTICLE

Capillary Flow Control in Nanochannel via Hybrid Surface

Ziran Ye,[a] Shunbo Li,[b] Cong Wang,[a] Rong Shen,[c] and Weijia Wen*[a]

Received 00th January 20xx,
Accepted 00th January 20xx

DOI: 10.1039/x0xx00000x

www.rsc.org/

We report a simple and effective approach to control the speed of capillary flow in nanochannel in a quantitative manner. Hydrophobic surface patterns were fabricated on both top and bottom walls of hydrophilic nanochannel to reduce the speed of fluid. Capillary flow speed can be precisely controlled in nanochannel by modifying the hydrophobicity ratio due to the flow characteristics on hydrophobic/hydrophilic surfaces. Without any additional energy source and equipment, this phenomenon can be realized solely by the wetting property of the patterned surface. We attribute this achievement to the significant surface effect on the liquid behavior due to the extremely large surface-to-volume ratio in nanochannel. This flow control method is helpful to obtain a detailed and thorough understanding of the dynamic filling behavior of capillary flow at nanoscale, as well as applicable to a wide variety of nanofluidics-based analysis systems.

Introduction

Controlling liquid in miniaturized devices has received enormous attention due to its utmost importance in chemical, biological and medical applications.[1-3] The precise manipulation of small amount of liquid in microfluidic, and recently nanofluididic system has been significantly extended.[4-6] Apart from those active controls such as mechanical pumping,[7] electrowetting[8] and electro-osmotic force[9] which need additional equipments or energy sources, capillary action, a ubiquitous phenomenon in nature caused by surface tension effects, affects the transport of liquids as a passive control method in various systems.

Capillary flow has been explored in a number of contexts, classical Washburn formula[10] gives the position of the moving meniscus x as a function of time t, which is known as a well-established model to describe the filling dynamics in capillaries:

$$x = \sqrt{\frac{\gamma \cos(\theta) h t}{3\eta}}, \qquad (1)$$

where γ is the surface tension of the liquid in air, θ is the contact angle of the liquid to the channel walls, h is the channel depth, and η is the liquid viscosity. However, in all reported experiments when the channel hydraulic diameter approaches tens of nanometers, the flow is found to be slower than that predicted by the Washburn model.[11] This deviation is mostly attributed to the electro-viscous effect,[12-13] air bubble formation[14] and the inconstant contact angle caused by the prevailing instantaneous force balance[15]. While the exact mechanisms responsible for the reduction in the flow rate may not be fully understood, previous studies have shown that the Washburn model overestimates the meniscus position and the actual speed during the filling process.[16, 17]

Capillary action is particularly prominent in nanochannels due to the large surface-to-volume ratio, and a number of works investigated the capillary filling influenced by introducing external power sources.[18, 19] However, there has been few report regarding the passive control of capillary flow in nanochannel, although it is intensively required in versatile micro/nanofluidic analysis systems which need a sufficient incubation time or reaction time. The difficulty may originate from the coexistence of multiple phases and the reduction in dimension comparing with microchannel in which internal geometric obstacles may be employed to block the flow.[20] Moreover, redesigning the dimensions of nanochannel to adjust the capillary filling speed is rather complicated and ineffective in nanofabrication. On the other hand, the surface property becomes crucial due to the large surface-to-volume ratio, and the instantaneous force balance caused by surface wettability prevails during capillary filling. Therefore, in this paper, we present an approach of controlling capillary flow by coating alternating hydrophobic/hydrophilic patterns on the top-bottom walls of nanochannel. Hybrid surface with different wettabilities plays a vital role in the autonomous capillary filling due to the flowing characteristics on hydrophobic/hydrophilic areas.

In general, fluid flow in nanochannel can be explained in terms of energy changes in the solid-liquid-gas system.[1] The total interfacial energy of the system, U_T, can be determined as follows:

$$U_{\mathrm{T}} = \sum_{\mathrm{i,j,k}} (\mathrm{A}_{\mathrm{S_jL_i}} \gamma_{\mathrm{S_jL_i}} + \mathrm{A}_{\mathrm{S_jG_k}} \gamma_{\mathrm{S_jG_k}} + \mathrm{A}_{\mathrm{L_iG_k}} \gamma_{\mathrm{L_iG_k}}) \qquad (2)$$

[a] Department of Physics, The Hong Kong University of Science and Technology, Clear Water Bay, Kowloon, Hong Kong
[b] School of Chemistry, University of Leeds, Woodhouse Lane, Leeds, LS2 9JT, UK
[c] Institute of Physics, Chinese Academy of Sciences, Beijing, China
* Corresponding Author: phwen@ust.hk

Electronic Supplementary Information (ESI) available: Depth profile of nanochannel measured by profilometer and the characterization of the hydrophobic/hydrophilic patterned surface

where $A_{S_jL_i}$, $A_{S_jG_k}$, and $A_{L_iG_k}$ are solid j- liquid i, solid j- gas k, and liquid i- gas k interface areas, and $\gamma_{S_jL_i}$, $\gamma_{S_jG_k}$, and $\gamma_{L_iG_k}$ are their corresponding surface energies per unit area, respectively. The classical Young's equation expresses the relationship between the surface energies and the liquid contact angle $\theta_{C_{ijk}}$ at the solid-liquid-gas interface line as:

$$\gamma_{S_jG_k} = \gamma_{S_jL_i} + \gamma_{L_iG_k}\cos\theta_{C_{ijk}} \quad (3)$$

To draw the pressure inside the fluid in nanochannel, *P*, as a function of the liquid volume V_L, we substitute the expression in eq (3) into eq (2), then the pressure *P* inside the capillary flow can be expressed as:[20]

$$P = -\frac{dU_T}{dV_L} = \sum_{i,j,k}\left(\frac{dA_{L_iG_k}}{dV_L} - \cos\theta_{C_{ijk}}\frac{dA_{S_jL_i}}{dV_L}\right) \quad (4)$$

We here define θ_1, θ_2 and θ_3 as the liquid contact angles to the bottom surface, top surface and hydrophobic patterns, respectively. According to eq (4), if the surfaces in nanochannel are completely hydrophilic, the pressure in the capillary flow, P_1, can be written as:

$$|P_1| = \frac{\gamma}{h}(\cos\theta_1 + \cos\theta_2 - \frac{2h}{w}), \quad (5)$$

where γ is the surface energy of the liquid, *h* is the depth of nanochannel.

To control the capillary filling in a quantitative manner, we hereby define a parameter, *R*, which is the ratio of hydrophobic area to the whole top-bottom surfaces in nanochannel:

$$R = \frac{n\pi r^2}{2wL} \quad (6)$$

where *n* is the number of hydrophobic patterns, *r* is the radius of each hydrophobic dot, *w* is the width, and *L* is the length of the nanochannel.

When the liquid meets the patterned surface in nanochannel, the resulting average wettability of the hybrid surface has a strong effect on the pressure in the liquid. In this case, the pressure can be determined by introducing eq (6) into eq (4) as the following:[20]

$$|P_2| = \frac{\gamma}{h}(\cos\theta_1 + \cos\theta_2 + (\cos\theta_3 - \cos\theta_1)R - \frac{2h}{w}) \quad (7)$$

The absolute value of pressure drop $\Delta P = |P_2| - |P_1| = \gamma/h(cos\,\theta_3 - cos\,\theta_1)R$ is negative due to R ranges from 0 to 1 and $(\cos\theta_3 - \cos\theta_1)$ is negative, thus the absolute value of pressure $|P_2|$ is smaller than $|P_1|$.

Since the pressure is actually negative inside the fluid in nanochannel, larger absolute value of pressure represents the larger drag force to the liquid. Therefore, $|P_2|$ is smaller than $|P_1|$ indicates the reduced drag force caused by the hydrophobic/hydrophilic surface pattern, resulting in the speed reduction in capillary flow. In addition, the expressions of pressure drop ΔP explicitly indicate that the capillary speed in nanochannel decreases with the reduced *h* and increased *R*. Taking advantage of this effect, it is possible that the speed of capillary flow in nanochannel can be controlled by implementing hydrophobic/hydrophilic surface patterns with appropriate *R*.

Experimental

In our experiment, silicon and glass wafers are employed as the top and bottom walls of the nanofluidic chip, which incorporates two connected channels in different geometries denoted as Channel A and Channel B, respectively. Channel A is designed to fabricate patterned nanochannel for capillary flow using standard photolithography technique, whereas Channel B will serve as the alignment mark for the hydrophobic pattern in Channel A. The flow chart in Fig. 1 illustrates the fabrication process.

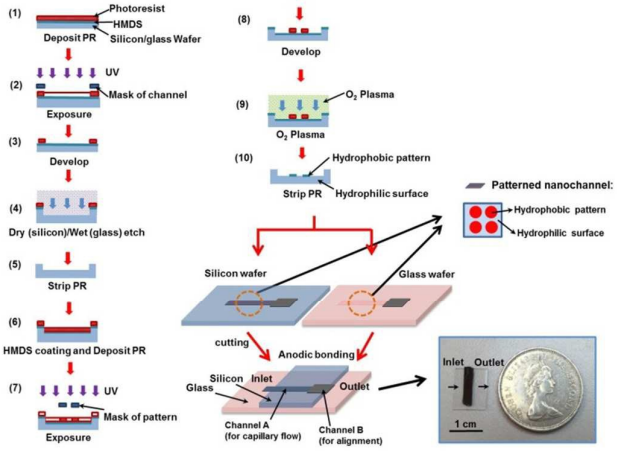

Fig. 1 Schematic illustration of the fabrication process of nanofluidic chip including photolithography, dry/wet etching, pattern coating, aligned anodic bonding and oxygen plasma treatment. The inset exhibits the optical image of the nanofluidic device for capillary flow.

A cleaned Silicon wafer was spin-coated by photoresist (PR) HPR 504 at 4000 rpm for 30 s. The wafer was then transferred to Mask Aligner (SUSS Microtec MA6-2, Garching, Germany) for 5 s exposure, followed by developing in FHD-5 developer for 60 s and post-baked on a hot plate at 120 °C for 1 min. Channel A (length of 2mm, width of 30μm) and Channel B (length of 2mm, width of 200μm) were dry-etched on a smooth silicon wafer with a uniform depth of 97nm (measured by profilometer, see Fig. S1 in Supplemental Materials) by a DRIE machine (Surface Technology systems, Newport, United Kingdom). After the PR stripping by oxygen plasma PS210 Photoresist Asher (PVA Tepla AG, Kirchheim, Germany) for 25 min, hexamethyldisilazane (HMDS) vapor priming was applied for 10 min to make the silicon wafer hydrophobic. After that, a second photolithography process was then conducted to transfer a series of hydrophobic patterns to channel A. Hydrophobic patterns with diameter of 3μm dot array on both silicon and glass was designed to induce instability to slow down the capillary flow. We chose several different values of *R* in our design, with *R*=0, 0.11, 0.23, and 0.31 respectively. Oxygen plasma treatment was performed for 1 min to make the exposed area hydrophilic. Afterwards, the PR was removed

by acetone in an ultrasonic bath for 5 min, and thus the resulting hydrophobic patterns on Channel A were achieved. The glass wafer was processed similarly to silicon wafer using photolithography technique. It is noted that only Channel B was wet-etched in the first step by buffered oxide etchant (BOE) for 6 min with the resulting channel depth of 170nm. Hydrophobic pattern was then precisely coated on the relative location of Channel A in the second step. After careful alignment under microscope (Olympus SZX16, Tokyo, Japan) with the reference of Channel B, silicon wafer and glass wafer were bonded together using anodic bonding technique to form a well-sealed nanofluidic device. It is noted that the hydrophobic dots on silicon and glass were rigorously aligned in the sealed nanochannel. Fig. 2 shows the completed nanofluidic chip and the surface morphology with hydrophobic patterns in bonded nanochannel. The hydrophobic/hydrophilic patterned surface was further characterized through vapor condensation and evaporation processes. Hydrophobic patterns with diameter of 3um dot array were clearly distinguished on hydrophilic surface, which indicates the successfully fabrication of the patterns. More details can be found in Fig.S2 in the supporting information.

To verify the controlling effect of the liquid filling speed in patterned nanochannel, the nanofluidic chip was placed horizontally, and a droplet of 5μL DI water dyed with Rhodamine B (10^{-2} M, Sigma-Aldrich, USA) was gently placed at the entry of nanochannel (Channel A) using a pipette. The fluid was immediately drawn into the nanochannel by capillary action and then flowed through the whole channel until it reached the exit. The change in the moving meniscus position was recorded over time at a rate of 2 frames per second using an inverted optical microscope (Olympus IX71, Tokyo, Japan) and recorded by a CCD camera (Olympus DP73, Tokyo, Japan). A sketch of this process in our experiment is also depicted in Fig. 2.

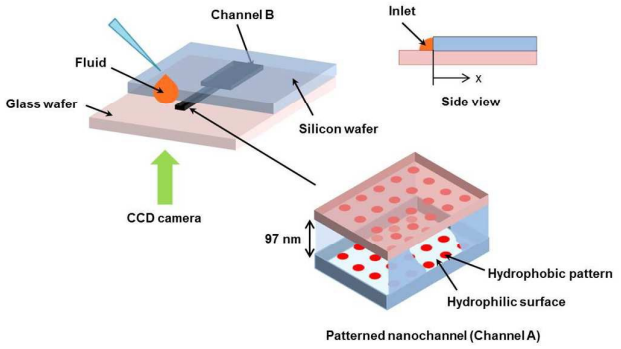

Fig. 2 Schematic illustration of nanofluidic chip in experiment with the side view and the configuration of patterned nanochannel. Hydrophobic patterns on the top and bottom hydrophilic walls were carefully aligned after anodic bonding process (not drawn to scale).

Results and Discussion

The images collected from experiments were analyzed using ImageJ software to measure the position of the meniscus as a function of time. The filling rate of the florescent fluid was measured. Fig. 3 exhibits the variation of the capillary meniscus position versus the square root of the filling time in nanochannel with various *R*, theoretical results for hydrophilic nanochannel calculated by eq (1) are also presented for comparison purposes.[11] It is noted that a systematic deviation from the behavior predicted by the Washburn formula is observed, as the slope in our experiment is much smaller than that in theoretical prediction. This is attributed to electroviscosity and variations in the dynamic contact angle as we have discussed earlier[11, 16, 17]. According to Fig. 3, the meniscus position is linearly related to the square root of the filling time in all cases, however the slope of the curve decreases with the increasing value of *R*.

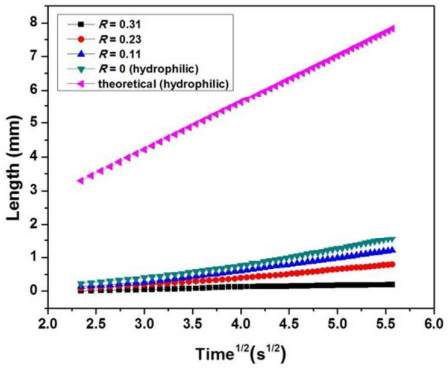

Fig. 3 Variation of meniscus position versus square root of filling time in nanochannel with different values of *R*. Theoretical results for hydrophilic nanochannel are also presented for comparison.

We further determine the slopes a of the curve $x = a\sqrt{t}$ in eq (1) to investigate the influence of the patterns on capillary flow in patterned nanochannel with different *R*. The relationship between the slope in Fig. 3 and *R* was investigated and five repeat attempts were made for each *R*, which is shown in Fig. 4. As *R* increased from 0 to 0.31, the slope in eq (1) decreased from 0.43 to 0.06. On the other hand, the absolute elapsed time for capillary flow in our hydrophilic nanochannel (*R* = 0) was 38.3s, and for different values of *R*, the elapsed time delayed at the hydrophobic patterns was measured as well to show the quantitative control of the capillary flow. The results in Fig. 4 showed that the delaying time increased up to 187.4s when increasing hydrophobic pattern ratio to 0.31. The reduced slope and increased delayed elapsed time caused by hydrophobic pattern intuitively reflects the reduction of capillary filling speed, thus implicitly indicates the effective and controllable suppression of capillary flow.

The experimental results indicate that the presence of hydrophobic/hydrophilic patterns evidently influenced the capillary flow in nanochannel, and this observation is in accordance with our theoretical analysis. Since capillary flow is a passive fluid motion caused by surface tension and mainly

governed by Washburn formula, the flow rate decreases with increasing contact angle. We propose that, when the fluid passed through nanochannel with hybrid surface by capillary motion, the presence of hydrophobic patterns on hydrophilic surface would cause an increased effective contact angle comparing with completely hydrophilic surface, and thus effectively slow down the capillary flow.

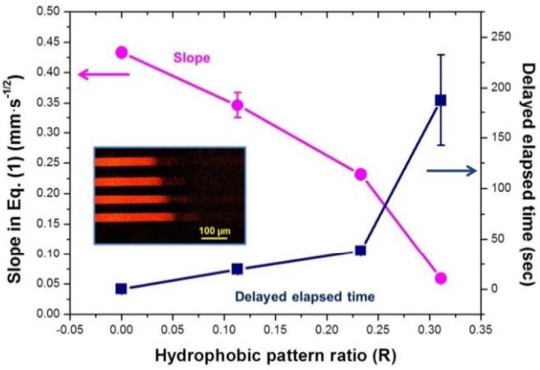

Fig. 4 Slope in eq (1) (pink dots) and delayed elapsed time to pass hydrophobic patterns (blue squares) with different hydrophobic pattern ratios. As an example, still images taken during capillary filling experiments in hydrophilic nanochannel were shown in the insert, with each time interval of 0.5s.

This method should be applicable in control of capillary flow in miniaturized analytical systems. For different channel dimensions, after the calibration of *R*, target speed of capillary flow can be obtained in nanochannel. The reaction time or incubation time in analytical nanodevices can thus be controlled repeatedly in a wide range. For the potential future work, decreasing nanochannel depth can further increase the domination of surface-related phenomena, and it is thus conceivable to meet more various requirement of filling speed in capillary flow. The limitation, however, may come from the difficulties in nanofabrication. In addition, electroviscous effect may further reveal itself in the fluid behaviour due to the double-layer overlap, and thus strongly account for the experimental results. Despite the discrepancy between the theoretical model and the experimental results, this control method showed the potential to control the speed of the autonomous capillary flow by a quantitative manner in a wide range.

Conclusions

In conclusion, a combination of photolithography and surface decoration technique is used to develop surface patterns on the top-bottom walls in nanochannel. The presence of hydrophobic patterns on the hydrophilic surfaces enables the containment of capillary flow, especially in nanochannel with large surface-to-volume ratio. By choosing appropriate hydrophobicity ratio, the filling speed of capillary flow in nanochannel can be controlled quantitatively without any additional manipulation. It is hence possible to satisfy various requirements of reaction or incubation time in biochemical application. These experimental results are of practical value, and such ability to control capillary filling speed in nanochannel holds promise for the successful control of fluid in a variety of nanofluidic analytical systems.

Acknowledgements

The authors would like to thank Dr. Lei Xu from Department of Physics, The Chinese University of Hong Kong for the helpful discussions. The authors wish to acknowledge the support of Hong Kong RGC grant (Grant No. AOE/P-02/12PG) and National Natural Science Foundation of China (Grant No. 11290165).

Notes and references

1 B. Zhao, J. S. Moore and D. J. Beebe, *Science*, 2001 **291**, 1023.
2 W. L. Hsu, D. W. Inglis, H. Jeong, D. E. Dunstan, M. R. Davidson, E. M. Goldys and D. J. E. Harvie, *Langmuir*, 2014, **30**, 5337.
3 R. Karnik, K. Castelino and A. Majumdar, *Appl. Phys. Lett*., 2006, **88**, 123114.
4 R. Qiao, and N. R. Aluru, *Appl. Phys. Lett*., 2005, **86**, 143105.
5 L. Xu, S. Davies, A. B. Schofield and D. A. Weitz, *Phys. Rev. Lett*., 2008, **101**, 094502.
6 L. Xu, A. Bergès, P. J. Lu, A. R. Studart, A. B. Schofield, H. Oki, S. Davies and D. A. Weitz, *Phys. Rev. Lett*., 2010, **104**, 128303.
7 M. A. Unger, H. P. Chou, T. Thorsen, A. Scherer and S. R. Quake, *Science*, 2000, **288,** 113-116.
8 M. W. Prins, W. J. J. Welters, and J. W.Weekamp, *Science*, 2001, **291**, 277.
9 R. Qiao and N. R. Aluru, Phys *Phys. Rev. Lett*., 2004, **92**, 198301.
10 E. W. Wasburn, *Phys. Rev*., 1921, **17**, 273.
11 S. Kelly, M. T. Balhoff and C. Torres-Verdín, *Langmuir*, 2015, **31**, 2167.
12 N. A. Mortensen and A. Kristensen, *Appl. Phys. Lett*., 2008, **92**, 063110.
13 J. Haneveld, N. R. Tas, N. Brunets and H. V. Jansen, *J. Appl. Phys*., 2008, **104**, 014309.
14 L. H. Thamdrup, F. Persson, H. Bruus and A. Kristensen, *Appl. Phys. Lett*., 2007, **91**, 163505.
15 Y. Zhu and K. Petkovic-Duran, *Microfluid. Nanofluid*, 2010, **8**, 275.
16 J.N. Kuo and W. K. Wang, *Microfluid. Nanofluid*, 2015, **18**, 57.
17 M. N. Hamblin, A. R. Hawkins, D. Murray, D. Maynes, M. L. Lee, A. T. Woolley, and H. D. Tolley, *Biomicrofluidics*, 2011, **5**, 021103.
18 N. R. Tas, M. Escalante, J. W. van Honschoten, H. V.Jansen and M. Elwenspoek, *Langmuir*, 2010, **26**, 1473.
19 V. N. Phan, N. T. Nguyen, C. Yang, P. Joseph, L. Djeghlaf, D. Bourrier and A. Gue, *Langmuir*, 2010, **26**, 13251.
20 J.W. Suk and J. H. Cho, *J. Micromech. Microeng*., 2007, **17**, N11.